Fundamental Research 4 (2024) 777–784

Contents lists available at ScienceDirect

Fundamental Research

journal homepage: http://www.keaipublishing.com/en/journals/fundamental-research/

Article

Ionic liquids inhibit the dynamic transition from α-helices to β-sheets in peptides

Ju Liu[a,c], Yanlei Wang[a,c,*], Feng Huo[a,b], Hongyan He[a,c,*]

[a] Beijing Key Laboratory of Ionic Liquids Clean Process, State Key Laboratory of Mesoscience and Engineering, CAS Key Laboratory of Green Process and Engineering, Institute of Process Engineering, Chinese Academy of Sciences, Beijing 100190, China
[b] Longzihu New Energy Laboratory, Zhengzhou Institute of Emerging Industrial Technology, Henan University, Zhengzhou 450000, China
[c] University of Chinese Academy of Sciences, Beijing 100049, China

ARTICLE INFO

Article history:
Received 30 May 2023
Received in revised form 14 December 2023
Accepted 15 December 2023
Available online 7 February 2024

Keywords:
α-β transition
Molecular dynamics simulation
Ionic liquids
Machine learning
Membrane channel protein

ABSTRACT

Abnormalities in the transition between α-helices and β-sheets (α-β transition) may lead to devastating neurodegenerative diseases, such as Parkinson's syndrome and Alzheimer's disease. Ionic liquids (ILs) are potential drugs for targeted therapies against these diseases because of their excellent bioactivity and designability of ILs. However, the mechanism through which ILs regulate the α-β transition remains unclear. Herein, a combination of GPU-accelerated microsecond molecular dynamics simulations, correlation analysis, and machine learning was used to probe the dynamical α-β transition process induced by ILs of 1-alkyl-3-methylimidazolium chloride ([$C_n$mim]Cl) and its molecular mechanism. Interestingly, the cation of [$C_n$mim]$^+$ in ILs can spontaneously insert into the peptides as free ions ($n \leq 10$) and clusters ($n \geq 11$). Such insertion can significantly inhibit the α-β, transition and the inhibiting ability for the clusters is more significant than that of free ions, where [C_{10}mim]$^+$ and [C_{12}mim]$^+$ can reduce the maximum β-sheet content of the peptide by 18.5% and 44.9%, respectively. Furthermore, the correlation analysis and machine learning method were used to develop a predictive model accounting for the influencing factors on the α-β transition, which could accurately predict the effect of ILs on the α-β transition. Overall, these quantitative results may not only deepen the understanding of the role of ILs in the α-β transition but also guide the development of the IL-based treatments for related diseases.

1. Introduction

α-helices and β-sheets are the main secondary structures of proteins [1–3], and the α-β transition is associated with the processes of signal transduction, membrane fusion, and the transcription and translation of genetic material [4–7]. The correct α-β transition is required for maintaining normal activity, e.g., Alzheimer's and Parkinson's syndromes are caused by an abnormal transition of amyloid in the brain from a structure with a high α-helix content to a structure with a high β-sheet content [8,9]. In addition, α-helices are highly stable biomechanical structures that are the basis of the material of the cytoskeleton, hair, and nails [10]. Silk fibronectin, which is rich in α-helices, has excellent toughness and tensile strength and is widely used in medical functional materials, including medical hydrogels and stents [11,12]. Therefore, the influence and mechanism of the α-β transition in proteins need to be better understood.

Considering the importance of the α-β transition, the molecular mechanism of the α-β transition and how to achieve precise regulation of the transition process is of interest in medicine, chemistry, biology, and materials science. Numerous experimental and theoretical studies of the α-β transition of proteins have been performed. Circular dichroism and chemical cross-linking studies have shown that coiled coils may be intermediate structures in the α-β transition [13]. Multi-scale analysis has indicated that the retractive elastic force in the α-β transition was not governed by entropy but was mainly the result of internal energy changes associated with conformational changes [14]. In general, the α-β transition can be easily regulated using external stimuli, such as the peptide concentration and pH [15–17]. Moreover, fluorinated amino acids have been shown to promote the conformational transition of a protein from an α-helix to a β-sheet [18]. These studies have preliminarily indicated the mechanism of the α-β transition and laid the foundation for further research.

Ionic liquids (ILs) have attracted great interest in life sciences, emerging as active drug ingredients [19–21], delivery agents [22,23], and antimicrobial agents [24] because of their excellent bioactivity and surface activity [25]. It has been shown that because of the hydrophobic and electrostatic interactions between ILs and proteins, ILs adsorb to protein surfaces [26], which would contribute to protein solubilization;

* Corresponding authors.
E-mail addresses: ylwang17@ipe.ac.cn (Y. Wang), hyhe@ipe.ac.cn (H. He).

https://doi.org/10.1016/j.fmre.2023.12.013

therefore, ILs can serve as storage media for proteins [27]. Furthermore, a combination of UV–Vis spectroscopy and molecular dynamics (MD) simulations has shown that ILs can modify the water structure on a protein surface to modulate the interfacial properties of the protein [28,29]. Importantly, ILs can alter the permeability and mechanical properties of cells [30], which can have impacts on the α-β transition. It can be concluded that ILs can directly or indirectly affect the structure and function of proteins, which in turn regulate cellular activity. However, the mechanism by which ILs affect the α-β transition is unclear because of the slow structural evolution between ILs and the α-β transition.

Molecular dynamics and machine learning have been employed for the recognition of protein secondary structures, relying on spectroscopic descriptors [31]. To elucidate the mechanism of the control of the α-β transition by imidazole ILs and to overcome the corresponding slow rate, all-atom μs-long steered molecular dynamics (SMD) simulations were performed with the help of graphics processing units (GPU) acceleration technology. We found that ILs inserted between the peptides in the form of free ions and ionic clusters, and the inserted ILs occupied the hydrogen bonding sites and reduced the number of hydrogen bonds (HBs) between the peptides, thus hindering the formation of β-sheets. The stretching rate (v), initial length (L_0), and surface charge of the peptides, together with the alkyl chain length (n) and cluster state of the ILs, affected the α-β transition. Finally, through machine learning, these descriptors were modeled using neural network algorithms, with Pearson correlation coefficient (r) reaching 0.951. These results will be useful for understanding the interaction process of ILs with proteins at the molecular level and for developing the application of ILs in disease treatment.

2. Models and methods

2.1. Atomic structures

We used the structural models of vimentin (1gk4), geminin (1uii and 1t6f), tumor suppressor protein (1deb), voltage-gated proton channel (3vmx), and leucine zipper (1zik). These α-helix-coiled coil proteins were immersed in a water solution with ILs at 0.136 mol/L. The PACKMOL package was used to build the initial configuration [31]. As shown in Fig. 1a, the typical ILs, 1-alkyl-3-methylimidazolium chloride, namely, [$C_n$mim][Cl] (n = 4, 6, 8, 10, 12, 14, 16), were used because they are widely used in biomedicine and materials science [32,33]. The size of the simulated system was approximately 5.1 nm × 5.1 nm × 29.7 nm. The periodic boundary condition was applied in three directions.

All simulations were performed via GPU-accelerated Amber18 using a timestep of 2 fs [34]. The protein.ff14SB force fields were used for peptides, and the general amber force field was adopted to describe the interaction within the ILs [35,51]. Water molecules were described by transferable interatomic potential with a three-point model (TIP3P) [36]. Non-bonding interactions included electrostatic and van der Waals forces, where the long-range Coulombic interaction was computed using the particle-mesh-Ewald algorithm [37], and the van der Waals force was described using the Lennard-Jones potential with a cutoff of 1.0 nm. The Lorentz–Berthelot mixing rules were used to model the parameters between different atom types, and the SHAKE algorithm was used to reduce high-frequency vibrations of hydrogen [38,52]. The Berendsen thermostat [39] and Berendsen barostat [40] were used to fix the temperature at 310 K and control the pressure at 1 bar with a coupling constant of 1.0 ps. The system was first equilibrated at 310 K and 1 bar in the NPT (constant-pressure, constant-temperature) ensemble for 50 ns. After equilibration, each structure was stretched in the NVT (canonical) ensemble by SMD. The two Cα atoms at the left end of the peptide were fixed to a harmonic spring, with a spring constant of 2 kcal/mol/A^2, while the two Cα atoms at the right end of the peptide were linked to a harmonic spring, with a spring constant of 10 kcal/mol/A^2. The springs were pulled at different speeds (v = 0.02–0.4 m/s) along the axial direction, $\varepsilon = \Delta L/L_0$, where ΔL is the tensile strain and L_0 is the initial end-to-end length of the peptide. For each peptide, the stretching simulations were repeated at least five times.

2.2. Correlation analysis

Correlation analysis was performed using the Statistic Package for the Social Science (SPSS) to correlate the stretch velocity (v), the characteristics of the peptides [the initial length of the peptide (L_0) and the negatively charged (P_{neg}) and the non-polar (P_{non}) amino acid content of the peptide] and the state of the ILs [alkyl chain length (n) and the proportion of large clusters ($P_{M \geq 16}$) and free ions ($P_{M = 1}$)] for the maximum β-sheet formation ($P_{\beta\text{-max}}$).

2.3. Model training

The model training used Scikit-learn [41] and TensorFlow [42]. The dataset contained 29 IL–peptide complexes, randomly divided into two groups: 80% for model training and 20% for model testing. A neural network algorithm [43] was used for mapping descriptors to the target $P_{\beta\text{-max}}$. The neural network consisted of one input layer, four hidden layers, and one output layer. The four hidden layers each contained 64, 64, 128, and 64 neurons, respectively; and the rectified linear unit activation function was used for each hidden neural network layer [44].

3. Results and discussion

3.1. Dynamical stretching behavior of the α-β transition in proteins

Proteins play essential roles in cellular metabolism, and during metabolism, cells generate tensile forces that induce α-β transitions. To simulate the force applied by the cells, a peptide was placed horizontally and a 2 kcal/mol/A^2 constraint was applied to the left end, and a harmonic spring of 10 kcal/mol/A^2 was applied to the right end, which was used to make the peptide stretch uniformly (Fig. 1a). The main sub-level bonds maintaining α-helices are intra-chain HBs, while the main sub-level bonds that maintain β-sheets are inter-chain HBs (Fig. 1b). Under tensile force, the intra-chain HBs break, leading to the decomposition of the α-helices and the formation of a disordered peptide conformation. Next, the disordered peptide self-assembles to form β-sheets under the interaction of inter-chain HBs.

Considering the stretching speed appreciably affects the transformation process [45], we first used different speeds (v = 0.02–0.4 m/s) to stretch the peptide at physiological saline concentrations. This stretching allowed the peptide (pdb: 1gk4) to deform and force-strain (f-ε) curves were obtained (Fig. 1c), where $\varepsilon = \Delta L/L_0$, and L_0 is the initial length of the peptide, and ΔL is the tensile strain. As the speed was reduced, the f-ε curve shifted downward as a whole, and the curve converged when v = 0.04 m/s. The tensile process can be divided into three stages [46]. The first stage ($0 \leq \varepsilon \leq 0.2$) was the elastic deformation phase, where the peptide underwent elastic deformation, f increased linearly with ε and satisfied the equation: $f = k_1\ \Delta\varepsilon$. The second stage was the plastic deformation phase ($0.2 < \varepsilon \leq 1.25$), f remained unchanged during the stretching process, f = 0.2 nN. The force f in the plastic phase had a linear relationship with the logarithm of the stretching velocity (ln$v$), which was in good agreement with previous work [45]. When ε continued to increase, $\varepsilon > 1.25$, the peptide underwent non-linear deformation, $f = k_2\ \Delta\varepsilon^2$.

Ramachandran plot analysis is a visual representation that reflects the secondary structure of a protein by calculating the distributions of the dihedral angles (ψ, φ) of the peptide backbone. We performed a Ramachandran plot analysis of the structures of the peptide before and after stretching (Fig. 1d) and found that the distribution of the dihedral angle of the peptide changed. Before stretching (ε = 0), the dihedral angles of the peptide were mainly distributed in the region “A”, corresponding to a high α-helix content; however, when ε = 1.25, the dihe-

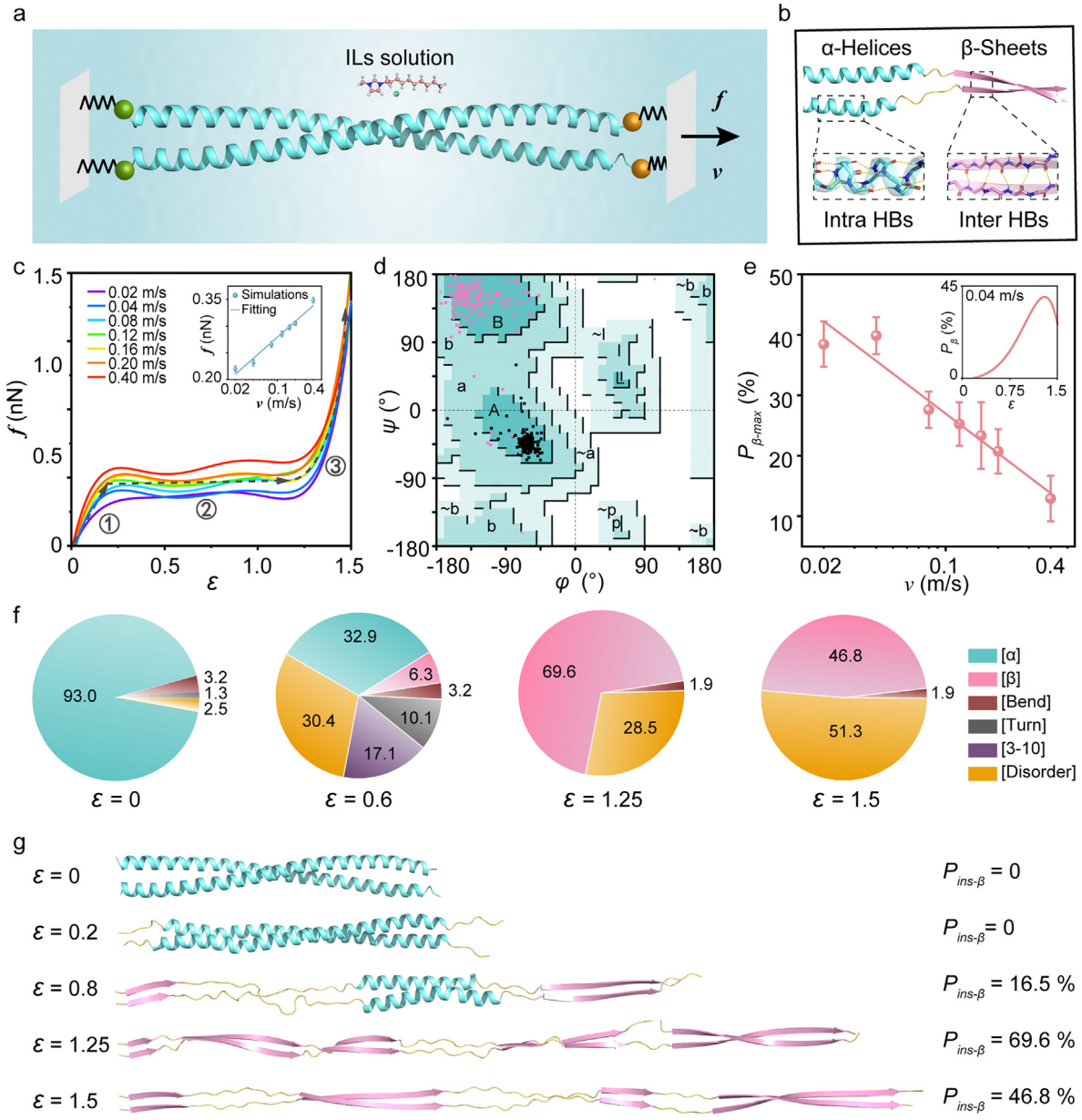

Fig. 1. (a) Model for studying the α-β transition. (b) Schematic diagram of α-helix and β-sheet. (c) Force f-strain ε curves of the peptide at different stretching speeds. The inset plots represent the relationship of f vs. ln$v$. (d) Dihedral angle distribution (Rasch diagram) of peptide before and after stretching using 1gk4 as an example. (e) The relationship between $P_{\beta\text{-max}}$ and ln$v$. The inset plots represent the content of β-sheet (P_β) as a function of strain for v = 0.04 m/s. (f) Evolution of the content of various secondary structures during stretching. (g) Simulation snapshots of the α-β transition during stretching.

dral angles were mainly distributed in region "B", corresponding to a high β-sheet content, indicating that stretching led to the transition of the peptide from an α-helix to β-sheet. The stretching process was also accompanied by the generation and decomposition of other secondary structures (Fig. 1f), the content of [Bend], [Turn] [3–10], and [Disorder] were 3.2%, 10.1%, 17.1%, and 30.4%, respectively, for ε = 0.6. These results also suggested that α-helix and β-sheet were the two most dominant secondary ordered structures (Fig. 1f); therefore, we recorded the content of β-sheet (P_β) and the maximum P_β ($P_{\beta\text{-max}}$) values during the stretching process (Figs. 1e, S1).

The P_β value increased overall as the stretching speed was reduced and converged at v = 0.04 m/s, which was consistent with the trend in the change of the f-ε curve with different values of v. Combined with the snapshots of the peptide during the simulated process (Fig. 1g), it was found that when ε reached 0.2, the stretching entered the plastic phase and β-sheets began to appear at both ends of the peptide, which was in complete agreement with the results observed for the stretching of horse hair [47]. The P_β value showed a trend of first increasing and then decreasing, and at all the different stretching speeds, β-sheet formation reached a maximum of approximately 1.25. For example, $P_{\beta\text{-max}}$ = 40.0% (ε = 1.25) at v = 0.04 m/s. Because we fitted and averaged the β-sheet curve, there was a difference between the $P_{\beta\text{-max}}$ value and the instantaneous content $P_{ins\text{-}\beta}$ = 69.1% (ε = 1.25). When entering the non-linear stretching phase, the β-sheets started to decompose from the middle of the peptide, with P_β = 27.2% (ε = 1.5). Thus, the stretching led to the rearrangement of HBs and dihedral angles to achieve the transition from α-helix to β-sheet in the peptide, and v = 0.04 m/s was the appropriate stretching speed. Therefore, a stretching velocity of 0.04 m/s was used in subsequent simulations.

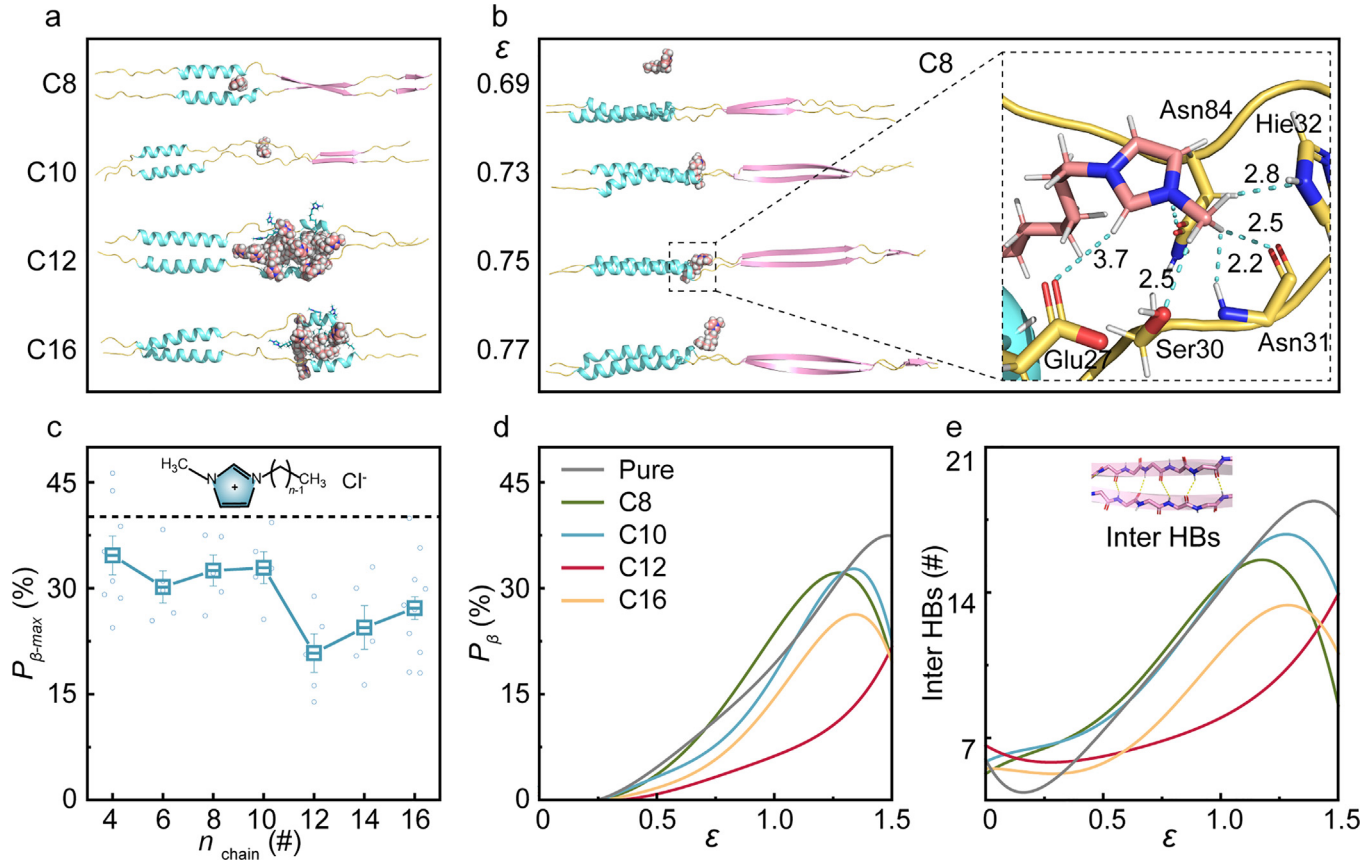

Fig. 2. (a) Simulation snapshots of the insertion of ILs with different alkyl chain lengths between peptides. (b) Insertion process for the $[C_8mim]^+$ free ion. (c) β-Sheet maxima of peptide 1deb after treatment with ILs with different chain lengths. (d, e) Content of β-sheet (P_β) and the number of intermolecular HBs as a function of strain after addition of different ILs.

3.2. Molecular mechanism of the regulation of the α-β transition by ILs

To investigate the mechanism by which ILs regulated the α-β transition, we added 0.136 mol/L of imidazolium chloride ILs with different alkyl chain lengths $[C_n mim][Cl]$ (n = 4, 6, 8, 10, 12, 14, and 16) to the system (pdb:1deb) as shown in Fig. 2a. The results indicated that ILs spontaneously inserted between the peptides as free ions or clusters. For ILs with short alkyl chains ($n \leq 10$), the ILs mainly inserted between the peptides vertically in the free ion state (Fig. 2b). When the alkyl chain had greater than 10 carbons, ILs mainly inserted between the peptides in the form of clusters. The inserted ILs occupied the HB sites between the peptides and formed a complex HB network with the peptides (Figs. 2b, S2). However, the inserted clusters not only occupied the HB sites but also made the peptide chain ectopic. These two different insertion modes resulted in different levels of inhibition of the formation of β-sheets during the α-β transition (Fig. 2c-d).

Compared with a pure water system ($P_{\beta\text{-max}}$ = 40.3%), the $P_{\beta\text{-max}}$ value decreased when ILs were added. For short-chain ILs ($4 \leq n \leq 10$) with predominantly free-ion insertion, the $P_{\beta\text{-max}}$ value was approximately 32%, while for the long-chain ILs ($n > 10$), which inserted mainly as clusters, the inhibition of β-sheet formation was more pronounced, for instance, $P_{\beta\text{-max}}$ = 20.8% for the IL with n = 12. The inserted ILs occupied HB sites between the peptides, reducing the number of HBs between the peptides (Fig. 2e), which in turn impeded β-sheet formation. The clusters occupied more HB sites and were more stable, compared with the free ions, which resulted in a stronger inhibition of β-sheet formation by ILs with long alkyl chains compared with ILs with short chains. However, different chain lengths of the ILs had little effect on the decomposition of the α-helix and the breaking of the intra-chain HBs (Fig. S3).

It is known that ILs are inserted between peptides in the form of free ions and clusters to hinder the formation of β-sheets during stretching. Because of the existence of extensive negatively charged and non-polar regions on the peptide surface (Fig. S4), the content of IL cations was enriched on the surface of the peptides, and this phenomenon became more pronounced with increasing alkyl chain lengths (Fig. S5). Hence, we analyzed the clustering of ILs with different alkyl chain lengths (Fig. 3). With the stretching of the peptide, the state of the ILs will change. The size distribution of the IL clusters in the system (Figs. 3b, S6) indicated that the proportion of free ions decreased with an increase in the alkyl chain length. For example, the proportion of free ions (M = 1) for ILs with n = 4, 10, and 16 under ε = 1.5 was 95.3%, 39.3%, and 0.0%, respectively. The content of small clusters ($5 \geq M \geq 2$) showed a trend of first increasing and then decreasing, for instance, the proportion of small clusters was 4.7%, 18.7%, and 6.0% for ILs with n = 4, 10, and 16 under ε = 1.5, respectively. In addition, medium-sized clusters ($15 \geq M \geq 6$) and large clusters ($M \geq 16$) also showed the same trend, and the proportions of medium and large clusters peaked for ILs with n = 14 and 12, respectively.

Interestingly, with increased stretching of the peptide, the clusters of $[C_8mim][Cl]$ dissociated, the proportion of small clusters ($5 \geq M \geq 2$) gradually decreased, and the proportion of free ions increased, $P_{M=1}$ = 59.7%, 67.3%, and 80.0% at ε = 0, 0.3, and 1.5, respectively (Fig. 3b). In detail, the number of ILs forming clusters on the surface of the peptide $N_{ILcluster}$ was 9 at ε = 0, and as ε increased, $N_{ILcluster}$ = 8 and 7 for ε = 0.9 and 1.5, respectively, and the small clusters were gradually dispersed. In contrast to $[C_8mim][Cl]$, there was clear cluster formation by ion aggregation for $[C_{12}mim][Cl]$, with a decrease in medium-sized clusters ($15 \geq M \geq 6$) and an increase in the proportion of large clusters. This result suggested that peptide stretch-

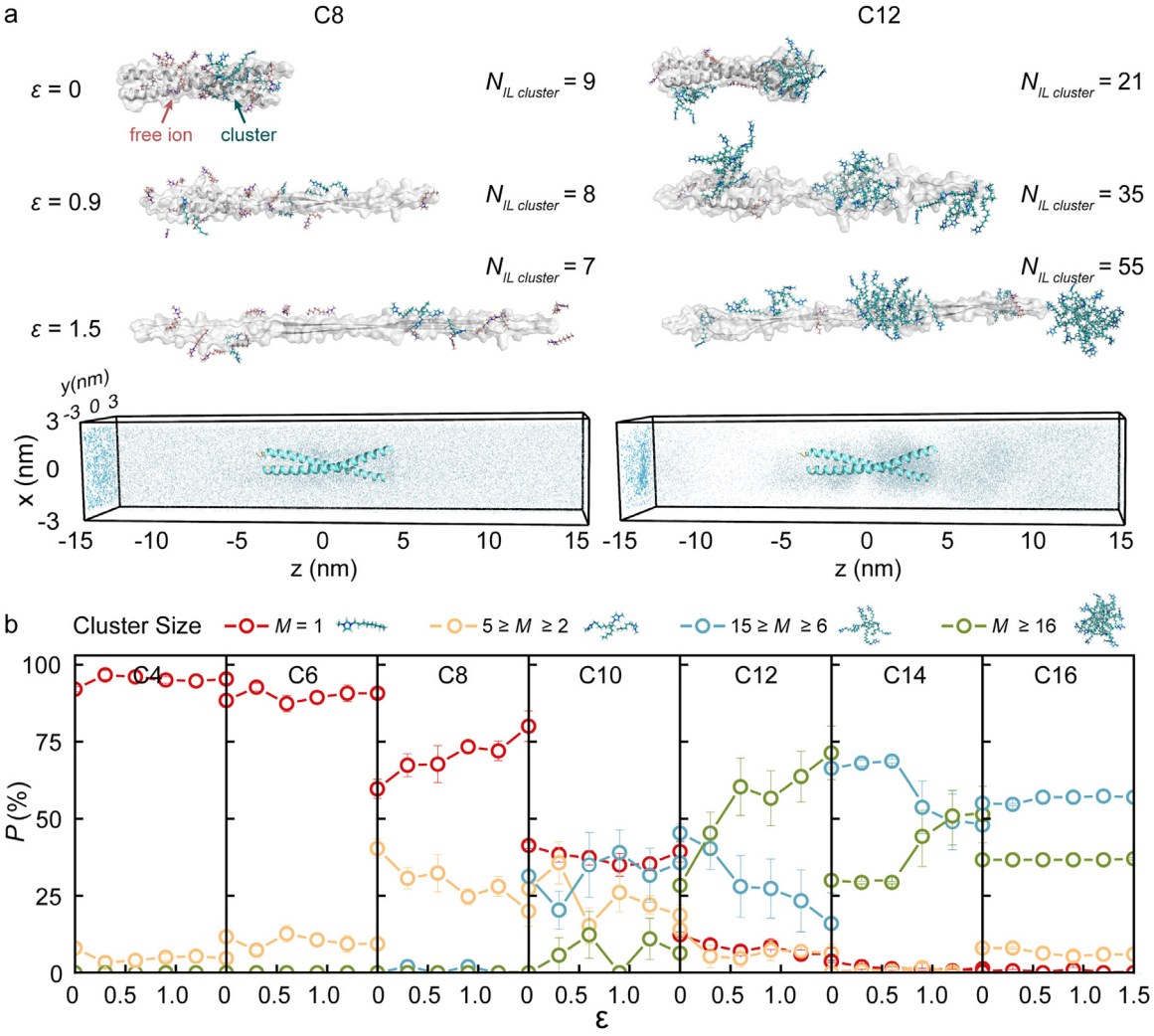

Fig. 3. (a) Simulation snapshots of the evolution of $[C_8mim]^+$ and $[C_{12}mim]^+$ clusters on the surface of peptides and trajectory density distribution of the cations. (b) The size distribution of the clusters in systems with ILs with different chain lengths.

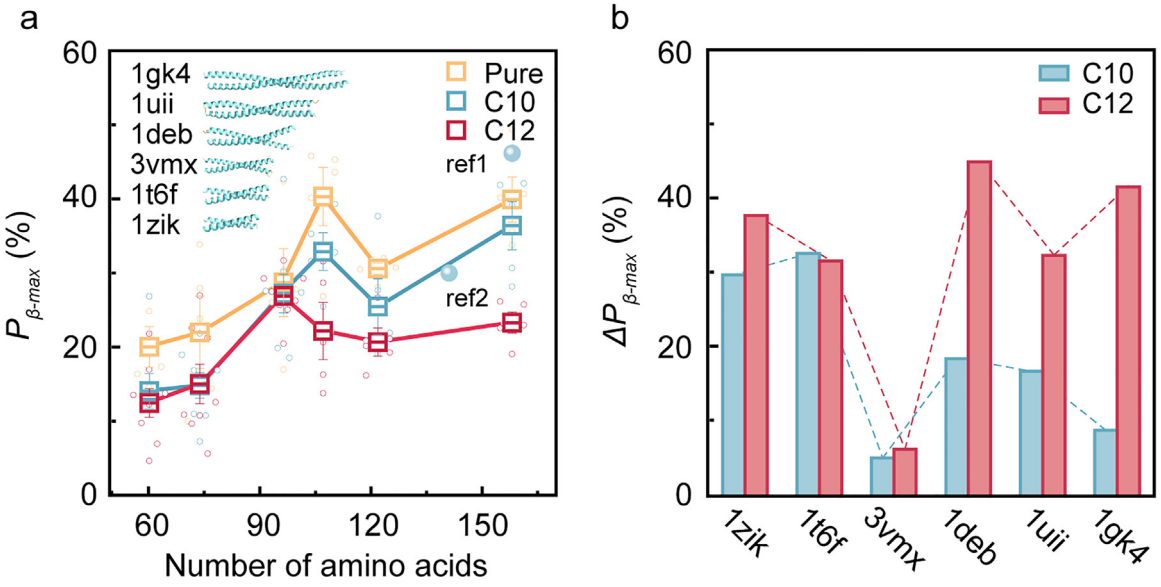

Fig. 4. (a) β-Sheet maxima ($P_{\beta\text{-max}}$) for peptides with different lengths. The PDB IDs of the peptides with length of 60, 74, 96, 107, 122, and 158 are 1zik, 1t6f, 3vmx, 1deb, 1uii, and 1gk4, respectively. Ref. [48] and ref. [49] represent literature $P_{\beta\text{-max}}$ values obtained by SMD simulations. (b) Reduction in $P_{\beta\text{-max}}$ values for ILs with n = 10 and 12.

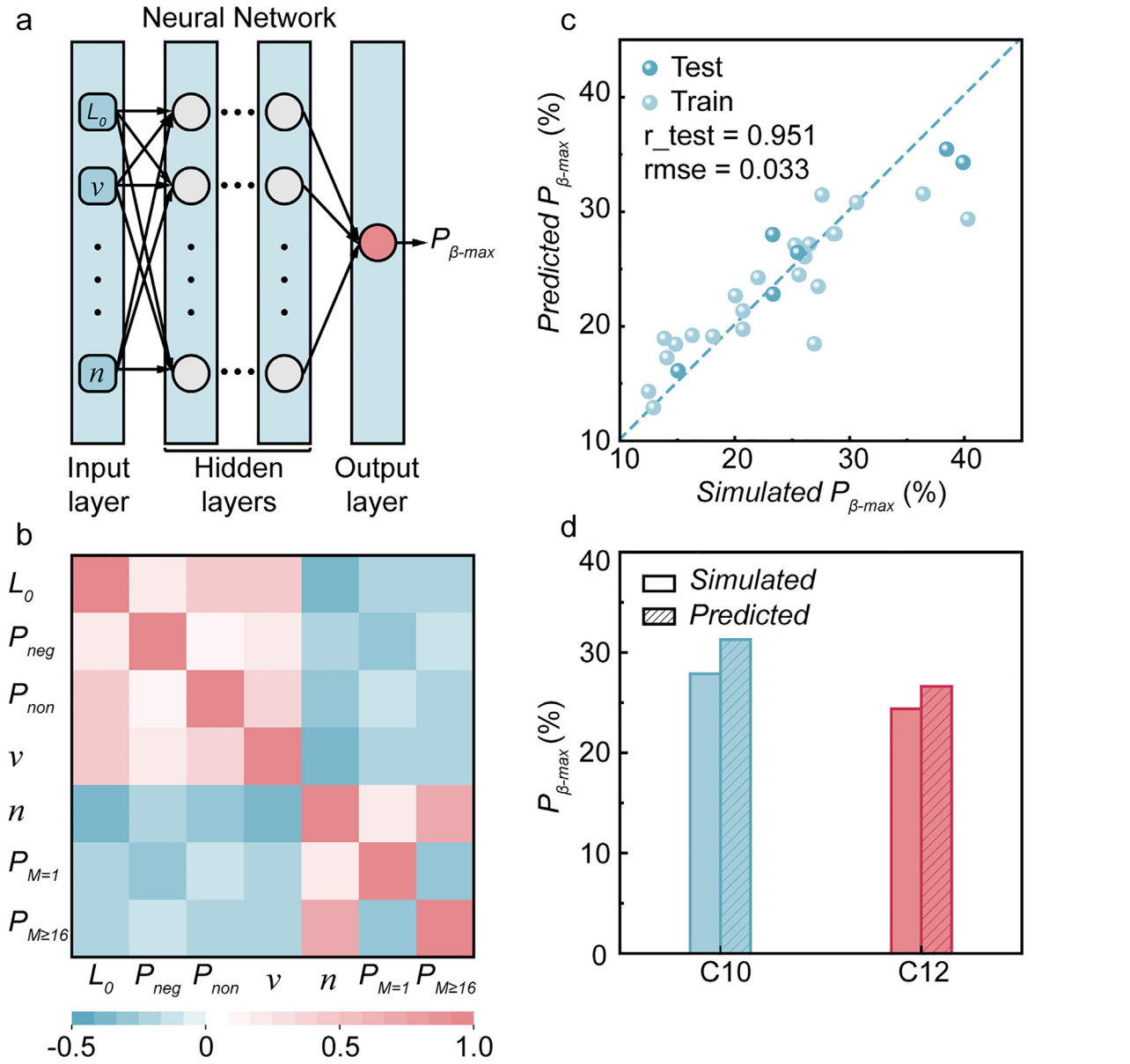

Fig. 5. (a) The architecture of the neural networks. (b) Heat map of the Pearson correlation coefficient (r) between the descriptors for predicting the values of $P_{\beta\text{-max}}$. (c) Prediction performance plots of the model for the α-β transition for the training and test sets: simulation vs. predicted $P_{\beta\text{-max}}$ values. The dashed line is the ideal 1:1 ratio. The Pearson correlation coefficient (r) and mean squared error (rmse) are for the test set. (d) The simulation and predicted $P_{\beta\text{-max}}$ values for the peptide (pdb:1gk4) in a water solution with ILs at 0.181 mol/L.

ing altered the interfacial clustering of ILs and transmitted this effect to the entire system.

From the above cluster analysis, we can correlate the cluster state of ILs with their ability to inhibit β-sheet formation. When $4 \le n \le 10$, the system was dominated by free ILs and mainly free ions were inserted between the peptides, resulting in less inhibition of β-sheet formation because relatively few HB sites were occupied by the free ions. When $12 \le n \le 16$, the ILs were inserted between the peptide chains as large clusters, the inserted IL clusters occupied more HB sites, the interaction was more stable, and the hindrance of β-sheet formation was greater, compared with ILs with $4 \le n \le 10$. For ILs with $12 \le n \le 16$, the proportion of large clusters decreased as n increased, and this decreasing trend coincided with a decrease in the ability of the ILs to inhibit β-sheet formation, demonstrating that the insertion of large clusters was the main reason why long chain ($12 \le n \le 16$) ILs hindered β-sheet formation. That is, the surface force of the peptide stretching drove a change in the interfacial state of the ILs, and in turn, the interfacial state of the ILs affected the transition process of the peptides.

3.3. Correlation analysis and machine learning-based predictive model of the α-β transition

To account for the effect of the initial length of the peptide (number of amino acids, N_0) on the α-β transition, we used peptides with different lengths in stretching experiments (Figs. 4a and S7–S10). The maximum value of the β-sheet content $P_{\beta\text{-max}}$ gradually increased with increasing values of L_0 in the control groups. For instance, the values for $P_{\beta\text{-max}}$ were 20.0%, 28.7%, and 40.0% for 1zik (N_0 = 60), 3vmx (N_0 = 96), and 1 gk4 (N_0 = 158), respectively, which was consistent with previous work [48]. However, 1deb (N_0 = 107) showed a higher $P_{\beta\text{-max}}$ because the formation of β-sheets was not only related to the peptide length but was also closely related to the type of amino acids and their arrangement

in the peptide. Furthermore, $[C_{10}mim][Cl]$, and $[C_{12}mim][Cl]$ both inhibited the formation of β-sheets during the transformation of different peptides. Hence, we also calculated the values for $\Delta P_{\beta\text{-max}}$, the reduction of the $P_{\beta\text{-max}}$ value by $[C_{10}mim][Cl]$ and $[C_{12}mim][Cl]$ (Fig. 4b). The effect of $[C_{12}mim][Cl]$ was more pronounced than for $[C_{10}mim][Cl]$ for all the peptides, which again indicated that inserted clusters had a greater effect on the α-β transition than free ions.

It can be concluded that the α-β transition was mainly influenced by the stretching velocity (v), the character of the peptides, including the initial length of the peptide (L_0), the negatively charged amino acid (P_{neg}), and non-polar amino acid ($P_{non,}$) content of the peptide (Fig. S11), and the states of the ILs including alkyl chain length (n), the proportion of large clusters ($P_{M \geq 16}$) and free ions ($P_{M = 1}$). Therefore, we selected these descriptors for a typical correlation analysis with $P_{\beta\text{-max}}$ and obtained the correlation equation given below (Fig. 5b).

$$U1 = 0.752L_0 - 0.757v - 0.361P_{M \geq 16} - 0.348n - 0.297P_{neg} - 0.151P_{non} - 0.058P_{M = 1} \quad (1)$$

$$U1 \propto 0.901P_{\beta-\max} \quad (2)$$

U1 was set as 1 and represents the factors affecting the transition. The positive or negative value of the correlation coefficient (R) represents the positive or negative correlation between the variables, and when $|R|$ is close to 1, the linear relationship is strong. As shown in Eq. 2, the value of R between *U1* and $P_{\beta\text{-max}}$ was 0.901, indicating that there was a significant correlation between *U1* and $P_{\beta\text{-max}}$. Therefore, combined with Eq. 1 where $R = 0.752$ between L_0 and *U1*, these results showed that L_0 contributed to the formation of β-sheets, while v and $P_{M \geq 16}$ distinctly inhibited the formation of β-sheets with R values of –0.757 and –0.297, respectively. The R of large clusters was larger than for free ions, indicating that large clusters had a significant effect on the formation of β-sheets. These results were in good agreement with our SMD simulations.

Machine learning was further used to predict the values for $P_{\beta\text{-max}}$, and the model was trained using the neural network algorithm (Fig. 5a), where the descriptors were selected from SMD simulations and typical correlation analysis. After 300 iterations, the loss functions of the training and test sets were < 0.005 as shown in Fig. S12. Finally, a Pearson correlation coefficient (r) of 0.951 was achieved for the test set (Fig. 5c), indicating that the model could accurately predict the effect of ILs on the α-β transition, although the plotted data clearly showed a slight overestimation at low values and an underestimation at high values, which is potentially because of the lack of data with an extremely high $P_{\beta\text{-max}}$ value accentuated by the fact that only four data points were originating from a $P_{\beta\text{-max}}$ value above 35%. This imbalance in the dataset led to an imbalance in the predictions [50]. Adding more data with high $P_{\beta\text{-max}}$ values could potentially reduce this effect. To test the generalization of our model, we used the model to predict the effect of 0.181 mol/L ILs with $n = 10$ and 12 on the α-β transition (Figs. 5d and S13), which was not considered in the previous dataset. Excitingly, the simulated values of $P_{\beta\text{-max}}$ for $n = 10$ and 12 were 27.9% and 24.4%, respectively, while the predicted values from the machine learning model were 31.3% and 26.7%, respectively. These results indicated that our model had a good generalization performance, especially considering the small sample size of the training set. It is worth noting that the selection of descriptors also has certain limitations. Our descriptors are solely derived from the MD simulations, which would restrain the applicability of the model. In the future, the property of ILs, the effect of concentration of ILs, and other descriptors related to α-β transition should be added to enhance the performance of the ML-based predictive model.

4. Conclusion

This work elucidated the mechanism by which ILs inhibit the α-β transition using a multi-technique investigation (SMD, correlation analysis, and ML). We demonstrated that stretching led to the rearrangement of HBs and dihedral angles in the peptide to achieve the transition from an α-helix to β-sheet. Upon the addition of ILs, the content of ILs was enriched on the peptide surface by electrostatic and hydrophobic interactions, and the interfacial clustering state of the ILs changed as the peptide stretched. Stretching led to the dissociation of $[C_8mim]^+$ clusters, as well as the formation of $[C_{12}mim]^+$ clusters. The inserted ILs occupied the HB sites and decreased the number of HBs between the peptides, thus, hindering the formation of β-sheets. Specifically, the inserted large clusters were a greater obstacle to β-sheet formation than the free ions, which can be attributed to the fact that the ionic clusters occupied more HB sites and interacted with the peptides more permanently, compared with the free ions, which caused misalignment of the peptides. Correlation analysis showed that the stretching speed (v) together with the characteristics of the peptide and the state of ILs affected the α-β transition. We also applied machine learning techniques to the proteins, showing that the neural network algorithm is a powerful tool for investigating the α-β transition. These results showing how ILs regulated the α-β transition will be useful in future medical research applications, including developing treatments for destructive neurodegenerative diseases, such as Parkinson's syndrome and Alzheimer's disease.

Declaration of competing interest

The authors declare that they have no conflicts of interest in this work.

Acknowledgments

This research was funded by the National Natural Science Foundation of China (21834006, 22078322, 21978293, and 21978027), the Youth Innovation Promotion Association of CAS (2021046, Y2021046), and State Key Laboratory of Treatments and Recycling for Organic Effluents by Adsorption in Petroleum and Chemical Industry (SDHY2114).

Supplementary materials

The details of steered molecular dynamics simulation and relevant data of ILs interaction with the peptides are provided in the Supporting Information.

Supplementary material associated with this article can be found, in the online version, at doi:10.1016/j.fmre.2023.12.013.

References

[1] M. Uhlen, L. Fagerberg, B.M. Hallstrom, et al., Tissue-based map of the human proteome, Science 347 (6220) (2015) 1260419.
[2] L. Pauling, R.B. Corey, H.R. Branson, The structure of proteins: Two hydrogen-bonded helical configurations of the polypeptide chain, Proc. Natl. Acad. Sci. 37 (4) (1951) 205–211.
[3] L. Pauling, R.B. Corey, The pleated sheet, a new layer configuration of polypeptide chains, Proc. Natl. Acad. Sci. 37 (5) (1951) 251–256.
[4] N. Amdursky, E. Gazit, G. Rosenman, Formation of low-dimensional crystalline nucleus region during insulin amyloidogenesis process, Biochem. Biophys. Res. Commun. 419 (2) (2012) 232–237.
[5] K.M. Pan, M. Baldwin, J. Nguyen, et al., Conversion of α-helices into β-sheets features in the formation of the scrapie prion proteins, Proc. Natl. Acad. Sci. 90 (23) (1993) 10962–10966.
[6] D.M. Rosenbaum, S.G.F. Rasmussen, B.K. Kobilka, The structure and function of G-protein-coupled receptors, Nature 459 (7245) (2009) 356–363.
[7] I. Aier, R. Semwal, U. Raj, et al., Comparative modeling and structure based drug repurposing of PAX2 transcription factor for targeting acquired chemoresistance in pancreatic ductal adenocarcinoma, J. Biomol. Struct. Dyn. 39 (6) (2021) 2071–2078.
[8] J.P. Taylor, J. Hardy, K.H. Fischbeck, Toxic proteins in neurodegenerative disease, Science 296 (5575) (2002) 1991–1995.
[9] S. Zhang, H. Dong, J. Bian, et al., Targeting amyloid proteins for clinical diagnosis of neurodegenerative diseases, Fundam. Res. 3 (4) (2023) 505–519.
[10] L. Pauling, R.B. Corey, The structure of hair, muscle, and related proteins, Proc. Natl. Acad. Sci. 37 (5) (1951) 261–271.
[11] A.M. Hopkins, L. De Laporte, F. Tortelli, et al., Silk hydrogels as soft substrates for neural tissue engineering, Adv. Funct. Mater. 23 (41) (2013) 5140–5149.
[12] W. Xu, K. Yagoshi, T. Asakura, et al., Silk fibroin as a coating polymer for sirolimus-eluting magnesium alloy stents, ACS Appl. Bio Mater. 3 (1) (2020) 531–538.

[13] F. Fiumara, L. Fioriti, E.R. Kandel, et al., Essential role of coiled coils for aggregation and activity of Q/N-rich prions and PolyQ proteins, Cell 143 (7) (2010) 1121–1135.
[14] A. Miserez, P.A. Guerette, Phase transition-induced elasticity of alpha-helical bioelastomeric fibres and networks, Chem. Soc. Rev. 42 (5) (2013) 1973–1995.
[15] R. Xing, C. Yuan, S. Li, et al., Charge-induced secondary structure transformation of amyloid-derived dipeptide assemblies from beta-sheet to alpha-helix, Angew. Chem.-Int. Edit. 57 (6) (2018) 1537–1542.
[16] J. Li, X. Du, S. Hashim, et al., Aromatic-aromatic interactions enable α-helix to β-sheet transition of peptides to form supramolecular hydrogels, J. Am. Chem. Soc. 139 (1) (2017) 71–74.
[17] K. Pagel, S.C. Wagner, K. Samedov, et al., Random coils, β-sheet ribbons, and α-helical fibers: one peptide adopting three different secondary structures at will, J. Am. Chem. Soc. 128 (7) (2006) 2196–2197.
[18] U.I.M. Gerling, M. Salwiczek, C.D. Cadicamo, et al., Fluorinated amino acids in amyloid formation: a symphony of size, hydrophobicity and α-helix propensity, Chem. Sci. 5 (2) (2014) 819–830.
[19] K.S. Egorova, E.G. Gordeev, V.P. Ananikov, Biological activity of ionic liquids and their application in pharmaceutics and medicine, Chem. Rev. 117 (10) (2017) 7132–7189.
[20] X. Lv, K. Chen, G. Shi, et al., Design and tuning of ionic liquid-based HNO donor through intramolecular hydrogen bond for efficient inhibition of tumor growth, Sci. Adv. 6 (45) (2020) eabb7788.
[21] C. Chen, C. Chen, Y. Li, et al., Characterization of lipid-based nanomedicines at the single-particle level, Fund. Res. 3 (4) (2023) 488–504.
[22] H. Albadawi, Z. Zhang, I. Altun, et al., Percutaneous liquid ablation agent for tumor treatment and drug delivery, Sci. Transl. Med. 13 (580) (2021) eabe3889.
[23] A. Banerjee, K. Ibsen, T. Brown, et al., Ionic liquids for oral insulin delivery, Proc. Natl. Acad. Sci. 115 (28) (2018) 7296–7301.
[24] L. Zheng, J. Li, M. Yu, et al., Molecular sizes and antibacterial performance relationships of flexible ionic liquid derivatives, J. Am. Chem. Soc. 142 (47) (2020) 20257–20269.
[25] C.M. Hamadani, M.J. Goetz, S. Mitragotri, et al., Protein-avoidant ionic liquid (PAIL)-coated nanoparticles to increase bloodstream circulation and drive biodistribution, Sci. Adv. 6 (48) (2020) eabd7563.
[26] H. Chu, Q. Zhao, J. Liu, et al., Ionic liquid-based extraction system for in-depth analysis of membrane protein complexes, Anal. Chem. 94 (2) (2022) 758–767.
[27] A.P. Brogan, J.P. Hallett, Solubilizing and stabilizing proteins in anhydrous ionic liquids through formation of protein-polymer surfactant nanoconstructs, J. Am. Chem. Soc. 138 (13) (2016) 4494–4501.
[28] L. Bui-Le, C.J. Clarke, A. Bröhl, et al., Revealing the complexity of ionic liquid–protein interactions through a multi-technique investigation, Comm. Chem. 3 (1) (2020) 55.
[29] K.P. Ghanta, S. Mondal, S. Mondal, et al., Contrasting effects of ionic liquids of varying degree of hydrophilicity on the conformational and interfacial properties of a globular protein, J. Phys. Chem. B 125 (33) (2021) 9441–9453.
[30] P. Kumari, V.V.S. Pillai, B.J. Rodriguez, et al., Sub-toxic concentrations of ionic liquids enhance cell migration by reducing the elasticity of the cellular lipid membrane, J. Phys. Chem. Lett. 11 (17) (2020) 7327–7333.
[31] L. Martinez, R. Andrade, E.G. Birgin, et al., PACKMOL: A package for building initial configurations for molecular dynamics simulations, J. Comput. Chem. 30 (13) (2009) 2157–2164.
[32] Y. Wang, H. He, C. Wang, et al., Insights into ionic liquids: From Z-bonds to quasi-liquids, JACS Au 2 (3) (2022) 543–561.
[33] J. Liu, Y. Wang, C. Wang, et al., Thermodynamical origin of nonmonotonic inserting behavior of imidazole ionic liquids into the lipid bilayer, J. Phys. Chem. Lett. 12 (40) (2021) 9926–9932.
[34] D.A. Case, S.R. Brozell, D.S. Cerutti, et al., Amber 2018. University of California, San Francisco (2018).
[35] J. Wang, R.M. Wolf, J.W. Caldwell, et al., Development and testing of a general amber force field, J. Comput. Chem. 25 (9) (2004) 1157–1174.
[36] W.L. Jorgensen, J. Chandrasekhar, J.D. Madura, et al., Comparison of simple potential functions for simulating liquid water, J. Chem. Phys. 79 (2) (1983) 926–935.
[37] T. Darden, D. York, L. Pedersen, Particle mesh Ewald: An N·log(N) method for Ewald sums in large systems, J. Chem. Phys. 98 (12) (1993) 10089–10092.
[38] H.C. Andersen, Rattle: A, "Velocity" version of the shake algorithm for molecular dynamics calculations, J. Comput. Phys. 52 (1) (1983) 24–34.
[39] H.J.C. Berendsen, J.P.M. Postma, W.F. Vangunsteren, et al., Molecular dynamics with coupling to an external bath, J. Chem. Phys. 81 (8) (1984) 3684–3690.
[40] Y. Zhang, S.E. Feller, B.R. Brooks, et al., Computer simulation of liquid/liquid interfaces. I. Theory and application to octane/water, J. Chem. Phys. 103 (23) (1995) 10252–10266.
[41] F. Pedregosa, G. Varoquaux, A. Gramfort, et al., Scikit-learn: Machine learning in Python, J. Mach. Learn. Res. 12 (2011) 2825–2830.
[42] M. Abadi, P. Barham, J. Chen, et al., TensorFlow: A system for large-scale machine learning, in: Proceedings of the 12th USENIX Symposium on Operating Systems Design and Implementation, 2016, pp. 265–283.
[43] W.S. McCulloch, W. Pitts, A logical calculus of the ideas immanent in nervous activity, Bull. Math. Biophys. 5 (4) (1943) 115–133.
[44] X. Glorot, A. Bordes, Y. Bengio, Deep sparse rectifier neural networks, J. Mach. Learn. Res. (2011) 315–323.
[45] K.A. Minin, A. Zhmurov, K.A. Marx, et al., Dynamic transition from alpha-helices to beta-sheets in polypeptide coiled-coil motifs, J. Am. Chem. Soc. 139 (45) (2017) 16168–16177.
[46] A. Zhmurov, O. Kononova, R.I. Litvinov, et al., Mechanical transition from alpha-helical coiled coils to beta-sheets in fibrin(ogen), J. Am. Chem. Soc. 134 (50) (2012) 20396–20402.
[47] L. Kreplak, J. Doucet, P. Dumas, et al., New aspects of the alpha-helix to beta-sheet transition in stretched hard alpha-keratin fibers, Biophys. J. 87 (1) (2004) 640–647.
[48] Z. Qin, M.J. Buehler, Molecular dynamics simulation of the alpha-helix to beta-sheet transition in coiled protein filaments: Evidence for a critical filament length scale, Phys. Rev. Lett. 104 (19) (2010) 198304.
[49] T. Giesa, C.C. Perry, M.J. Buehler, Secondary structure transition and critical stress for a model of spider silk assembly, Biomacromolecules 17 (2) (2016) 427–436.
[50] A. Mansouri Tehrani, A.O. Oliynyk, M. Parry, et al., Machine learning directed search for ultraincompressible, superhard materials, J. Am. Chem. Soc. 140 (31) (2018) 9844–9853.
[51] B. Li, C. Wang, Y. Zhang, et al., High CO_2 absorption capacity of metal-based ionic liquids: A molecular dynamics study, Green Energy Environ. 6 (2) (2021) 253–260.
[52] Y. Shi, X. Zhao, Q. Liu, et al., Wetting sub-nanochannels via ionic hydration effect for improving charging dynamics, Green Energy Environ. 9 (3) (2024) 473–480.

Ju Liu has been a PhD candidate at the University of Chinese Academy of Sciences since 2019, specializing in the study of interactions between ionic liquids and biomembranes, as well as the effects of ionic liquids on the structure and function of membrane proteins. His research employs molecular dynamics simulations and machine learning techniques to elucidate the intricate mechanisms underlying these interactions. Through the investigation of the positioning and diffusion of ionic liquid molecules on membrane proteins, he aims to provide valuable insights into this field.

Yanlei Wang (BRID: 06331.00.22365) is a doctor/associate professor, Institute of Process Engineering, Chinese Academy of Sciences (IPE, CAS). He received his PhD in mechanical engineering from Tsinghua University in 2017, where he investigated the energy transport and storage process across low-dimensional materials and their interfaces. He started as an assistant professor at IPE, CAS in 2017 and became an associate professor there in 2019, where he is working on the fundamental studies of ionic liquid structure/property at the solid surface, diffusion-transport process in the nanoscale confined system, and charging-discharging mechanism of ionic liquid-based energy storage devices, etc.

Hongyan He (BRID: 03092.00.58585) is a professor, Institute of Process Engineering, Chinese Academy of Sciences (IPE, CAS). She mainly focuses on the study of green medium ionic liquids and chemical engineering processes. By integrating multiscale simulation and experimental characterization, she has developed several chemical thermodynamics models for interfacial ionic liquids and uncovered the correlation between the structure and performance of nanoscale confined ionic liquids. This supports cutting-edge applications such as efficient utilization of biomass, CO_2 capture and conversion, and evaporation-driven power generation. She has also served as Executive Editor of *Green Energy & Environment*, Advisory Board member of *ChemComm and Journal of Chemical & Engineering Data*, and youth editorial member of journals such as *The Innovation and Acta Physico-Chimica Sinica*.